Physica B 665 (2023) 415042

Contents lists available at ScienceDirect

Physica B: Condensed Matter

journal homepage: www.elsevier.com/locate/physb

The second, third harmonic generations and nonlinear optical rectification of the Mathieu quantum dot with the external electric, magnetic and laser field

Mustafa Kemal Bahar *, Pınar Başer

Department of Physics, Faculty of Science, Sivas Cumhuriyet University, 58140, Sivas, Turkey

ARTICLE INFO

Keywords:
Quantum dot
Laser field
Electric field
Magnetic field
Nonlinear optical properties

ABSTRACT

In this study, the nonlinear optical properties of the $In_xGa_{1-x}As/GaAs$ Mathieu quantum dot (MQD) are investigated for the first time, focusing on the nonlinear optical rectification (NOR), second harmonic generation (SHG), and third harmonic generation (THG). The effects of external fields such as the electric field, magnetic field, and laser radiation field on the nonlinear optical properties of MQD are examined, along with structural parameters such as quantum dot depth and width determined by the indium concentration. The motivation of the study is to explain the NOR, SHG, and THG characteristics of MQD in response to changes in external fields and structural factors. To investigate the effects of the laser field, the time-dependent part of the laser field is transferred to the potential energy term of the wave equation using the Kramers–Henneberger (KH) and dipole approximations, creating a laser-dressed potential. Then, the effective potential wave equation is solved using the tridiagonal matrix method. The effects of external fields and structural parameters of MQD on the NOR, SHG, and THG coefficients are discussed in detail. The optimality of the structure for device design and applications considering MQD is revealed, and alternative parameter analysis is conducted for this optimality.

1. Introduction

The quantum confinement effects in semiconductors have been extensively studied both experimentally and theoretically, and it has been shown that they have significant impacts on the electronic properties, such as absorption–emission and subband energies-binding energies, as well as on the optical and statistical properties. Low-dimensional structures such as quantum wells (QWs) (confinement in one dimension), quantum wires (QWWs) (confinement in two dimensions), and quantum dots (QDs) (confinement in three dimensions) can be obtained with the advancement of growth techniques, which restrict the motion of particles in semiconductor materials. This situation provides a good motivation to explore different confinement potentials theoretically. It has been calculated that the binding energies and oscillator strengths of the particles are larger than those in bulk materials. Furthermore, as the size decreases, it has been observed that the resonant frequencies in quantum dots shift towards the blue region. Along with the changes in linear optics, the low-dimensional effects of particles in small-sized materials lead to nonlinear optical (NLO) responses that involve new physical phenomena by enhancing their interaction with intense optical fields. NLO effects have enabled various applications, including optical switches and ultrafast laser pulse generation [1–5]. In optoelectronic technology, quantum dots (QDs), where particles are confined in all three dimensions, have garnered greater attention compared to other low-dimensional structures. The quantum effects are more pronounced in QDs because the electron wavelength is comparable to the confinement length [6]. The three-dimensional confinement of QDs leads to the formation of inter-layer optical transitions of dipole matrix elements. Therefore, QDs exhibit more pronounced nonlinear effects compared to quantum wires and wells [7,8]. Additionally, these structures have various advantages, such as improved thermal stability [9], insensitivity to back reflection [10], lower threshold current density [11], and ultra-narrow spectral linewidth, thanks to their atom-like discrete state density [12]. Similar to other low-dimensional structures, the form of the confinement potential of particles in quantum dots has a significant impact on the optical performance of the structure [13]. Hence, effective potentials for QDs can be considered in different forms such as parabolic, triangular, spherical, and double-ring [14–18]. Some experimental studies suggest that the most suitable quantum dot profiles for encompassing electrons should be well-like structures [19]. In line with these suggestions, the Mathieu functions have applications

* Corresponding author.
E-mail addresses: mussiv58@gmail.com (M.K. Bahar), pbaser34@gmail.com (P. Başer).

https://doi.org/10.1016/j.physb.2023.415042
Received 12 April 2023; Received in revised form 30 May 2023; Accepted 2 June 2023
Available online 16 June 2023

in various fields, including optics, quantum mechanics, and general relativity [20]. These functions arise in problems involving periodic motion or the analysis of boundary value problems for partial differential equations with elliptic symmetry [21–23]. Moreover, Mathieu differential equations are used in engineering, physics, and applied mathematics in diverse areas [24–31]. In this study, MQDs (Multiple Quantum Dots) consisting of GaInAs/InAs are investigated. GaInAs, a ternary semiconductor compound, is more advantageous in electronics and optoelectronics compared to other semiconductor compounds [32]. Additionally, at room temperature, the bandgap energy for $x = 0.47$ is 0.75 eV, which lies between the bandgaps of Ge and Si. This bandgap value of GaInAs is highly compatible with long-wavelength fibre optic communication [33]. The electron effective mass in GaInAs is $m^{\star}/m^{o} = 0.041$ [34]. Since effective mass is associated with energy–momentum, a low effective mass leads to high carrier mobility, resulting in higher carrier velocities and increased current carrying capacity. One of the primary applications of GaInAs semiconductor compound is infrared photodetectors in the wavelength range of $1.1\ \mu m < \lambda < 1.7\ \mu m$. Compared to photodiodes made of Ge, GaInAs photodiodes have advantages such as faster time response, higher quantum efficiency, and lower dark current for the same sensor area [35]. Similarly, GaInAs semiconductor lasers are an important application in optoelectronics. These lasers are widely used in chemical sensing and pollution control. GaInAs/InAlAs quantum well lasers [36], quantum cascade lasers (QCL) [37], and InGaAs quantum dot lasers on InAs [38] have been achieved. GaInAs lasers are used in triple-junction photovoltaics and also for thermophotovoltaic energy generation [39]. Additionally, HEMT (High Electron Mobility Transistor) devices obtained with InGaAs are one of the fastest transistor types [40].

External electric, magnetic, and laser fields applied to low-dimensional structures alter the symmetry and effective confinement potential of the structure. Many recent studies have shown that the optical properties change as the symmetry of the structure is broken [41–43]. In this context, external fields that change the symmetry of the structure can be considered as important arguments for controlling the electronic and optical properties of the structure. Therefore, numerous studies have been conducted to investigate the effects of electric, magnetic, and laser fields on the nonlinear optical and electronic properties of quantum systems [44–50]. Additionally, variations in structural parameters such as potential depth and width also affect the optical transitions. In this study, we also investigate the effects of structure parameters, such as the In concentration (x) that changes the potential depth and the parameter η associated with the potential width, along with external fields on the nonlinear optical properties of the MQD. While linear optics is applicable only at low power levels, high power is required for the occurrence of nonlinear optical phenomena, and nonlinear optical processes play an active role in many laser and optoelectronic device designs. This branch of optics is also important in areas such as ultra-short pulse transmission in fibre optics [51]. Nonlinear optics also explains the nonlinear response of properties such as polarization, frequency, wavelength, phase of the incident light, and interaction with different media. Some examples of such nonlinear interactions include the nonlinear optical reflection (NOR), second harmonic generation (SHG), and third harmonic generation (THG). Nonlinear effect refers to the nonlinear optical rectification defined as the formation of a DC or low-frequency polarization when intense light passes through a crystal. NOR provides a significant function for generating THz-level emissions using lasers [52]. SHG, as is well known, is a process in which an electromagnetic wave interacting with a nonlinear material produces a wave with twice the frequency of the incident wave. SHG production is a process used in laser sources [53], optical parametric amplifiers [54], as well as in the development of imaging and microscopy [55]. THG plays a fundamental role in the operation mechanism of optical devices such as light-emitting diodes and optical switches [56]. Due to such applications in technology, interest in nonlinear optical properties has increased.

The effect of a laser field on the electronic structure and nonlinear optical properties of a GaAs asymmetric double quantum dot has been investigated. From the obtained findings, it has been concluded that the electronic structure and optical properties are sensitive to the laser-dressed potential for certain values of structure parameters and under intense laser application, asymmetric double quantum dots are suitable heterostructures for THz-level NOR [57]. The presence of an external magnetic field has been theoretically studied for the cases with and without impurity atoms to investigate the SHG and THG characteristics of the quantum dot. It has been observed that SHG and THG increase and shift towards lower energies when an impurity term is present, and the magnitudes of SHG and THG increase with increasing magnetic field. However, with the increase in the magnetic field, their resonant energies shift to higher energies, and it has been determined that the structure parameters have significant effects on the SHG and THG of the QD [58]. The electronic properties and NOR characteristics of a spherical quantum dot with a parabolic confinement under an electric field containing a hydrogenic impurity have been investigated. It has been determined that as the electric field increases, the maximum value of the NOR coefficient increases, and the resonant peak points shift to lower photon energies [59]. External fields not only have significant effects on nonlinear optical properties such as NOR, SHG, and THG but also on other nonlinear optic properties such as total refractive index coefficients (TRICs) and total absorption coefficients (TACs). The electronic states and nonlinear optical properties of Y-shaped quantum dots have been studied under an electric field. It has been observed that the external electric field has a significant effect on energy levels, optical absorption coefficients, and refractive index. As the electric field increases, the resonance amplitudes of TACs decrease, while RICs increase their resonant amplitudes [60]. A vertically stacked QDs structure with two different potential profiles, Gaussian and Bessel, has been investigated for TACs and TRICs under the influence of a laser field. Interesting dependencies on laser parameters have been observed for the resonance frequency of the total AC. It has been found that even small values of laser parameters increase the amplitudes of ACs [61]. NOR, SHG, and THG characteristics are significantly influenced not only by external fields such as electric, magnetic or laser fields but also by Gaussian white noise. In other words, Gaussian white noise has a functional impact on the NOR, SHG, and THG processes. In this context, the effects of Gaussian white noise on the NOR, SHG, and THG of impurity-doped quantum dots have been extensively investigated [62–65]. The most important and common result of these noise studies is as follows: The presence and application method of noise are crucial for NOR, SHG, and THG. The peak intensities of the NOR, SHG, and THG profiles exhibit informity and sometimes promote photon resonance enhancement. These findings provide an important opportunity to adjust the NOR coefficient of impurity-doped quantum dot systems and utilize them in technology by employing noise. In this study, the effects of external parameters such as the laser field (α_0), electric field (ξ), and magnetic field (B), as well as structural parameters such as quantum dot depth and width, on the electronic and optical properties have been determined. Furthermore, it is important in terms of applications to provide a quantitative answer on how the optical properties can be adjusted by varying the external fields (α_0, ξ, and B) and appropriately tuning the structural parameters (x and η). The obtained findings revealed that NOR, SHG, and THG depend on the confinement of the quantum dot and the external parameters. These variables can be evaluated as alternatives to each other, taking into account factors such as optimality. Due to the possibility of experimentally producing such a potential within the confinement limitations in a well-like structure, the theoretical results obtained can be useful for practical applications.

The work is organized as follows. Section 2 presents the theoretical calculation procedure. In Section 3, the numerical results and comments on electronic properties and nonlinear optical coefficients are given, and finally in Section 4, the results obtained are provided.

2. Theoretical model and procedure

The time-dependent Schrödinger equation for the Mathieu quantum dot (MQD) generated by InGaAs/GaAs heterostructure, under the influence of the external electric, uniform magnetic and a linearly polarized laser radiation field is given by

$$\left[\frac{\mathbf{P}+e(\mathbf{A}(\mathbf{r},t)+\mathbf{A}_{mf}(\mathbf{r}))^2}{2m^\star}+V_{MQD}(r)+e\xi.\mathbf{r}\right]\Psi(\mathbf{r},t)=i\hbar\frac{\partial\Psi(\mathbf{r},t)}{\partial t}, \tag{1}$$

where $m^\star$ is the effective mass, V_{MQD} is the MQD potential, ξ is the external electric field strength. The laser radiation field relates to $\mathbf{A}(\mathbf{r},t)$ via $\mathbf{F}=\frac{\partial\mathbf{A}}{\partial t}$. F contains the electric and magnetic field components of the electromagnetic field. During considering the electromagnetic radiation field, in the Coulomb gauge, $\nabla.\mathbf{A}=0$ and scalar potential $\Phi(\mathbf{r}=0)$ are employed. $\mathbf{A}_{mf}$ is the vector potential of uniform magnetic field. For $\mathbf{A}_{mf}$ vector potential, $\mathbf{A}_{mf}=(1/2)(\mathbf{B}\times\mathbf{r})$ with $\mathbf{B}=(0,0,B)=(B_x,B_y,B_z)$ external uniform magnetic field along the $z-$axis is taken into consideration. Within the dipole approximation [66], the vector potential of the laser field is considered as linearly polarized along the $x-$axis with $\mathbf{A}(t)=A_0cos(\omega t)\hat{k}$, where $\hat{k}$ is the unit vector in the $z-$axis. It should be noted that the high frequency limit is taken into account in consideration of the laser radiation field [67]. Due to $\mathbf{A}(t).\mathbf{A}_{mf}(r)=0$ and the time-dependence of only laser field, the time-dependence of the laser field is changed from the kinetic energy term to the potential energy term by applying Kramers–Henneberger (KH) transformation [68,69]. Then, time-dependent Schrödinger equation converts to the following form:

$$\left[\frac{(\mathbf{P}+e\mathbf{A}_{mf}(\mathbf{r}))^2}{2m^\star}+V_{MQD}(r+\alpha(t))+e\xi r\right]\chi(\mathbf{r},t)=i\hbar\frac{\partial\chi(\mathbf{r},t)}{\partial t}, \tag{2}$$

where, $\chi(\mathbf{r},t)$ is an outcome of the KH operator. $\alpha(t)$ ensures transferring to the potential energy for the time dependence in the kinetic energy, and $\alpha(t)=\alpha_0 sin(\omega t)\hat{k}$ including $\alpha_0=eF_0/m^\star\omega^2$ where F_0 is the amplitude of the laser radiation field, while ω is the angular frequency of the laser radiation field. α_0 is the laser-dressing parameter in determining the laser field strength. In order to eliminate the time dependence in Eq. (2), the Fourier Floquet series [67] and Ehlotzky approach [70,71] are considered. Then, the wave equation is transformed to

$$\left[\frac{(\mathbf{P}+e\mathbf{A}_{mf}(\mathbf{r}))^2}{2m^\star}+\frac{1}{2}\Big(V_{MQD}(r+\alpha_0)+V_{MQD}(r-\alpha_0)\Big)+e\xi r\right]\psi(\mathbf{r})=E\psi(\mathbf{r}). \tag{3}$$

The polar coordinates ($x=rcos\phi$, $y=rsin\phi$) for the symmetry of the interaction system are appropriate. Considering the external uniform magnetic field ($\mathbf{B}=(\vec{B}_x,\vec{B}_y,\vec{B}_z)=(0,0,B\hat{k})$) and reasonable gauge transformation ($\mathbf{A}_{mf}(\mathbf{r})=(1/2)(\mathbf{B}\times\mathbf{r})$), the Hamiltonian of the system is obtained as

$$H=-\frac{\hbar^2\nabla^2}{2m^\star}+\frac{m^\star\omega_c^2}{8}r^2+\frac{\omega_c}{2}L_z+\frac{1}{2}\Big(V_{MQD}(r+\alpha_0)+V_{MQD}(r-\alpha_0)\Big)+e\xi r, \tag{4}$$

where ω_c is cyclotron frequency inside crystal as $\omega_c=eB/m^\star$ [72], L_z is $z-$component of the angular momentum operator as $L_z=-i\hbar\frac{\partial}{\partial\phi}$. In this case, the wave equation to be solved is $H\psi(\mathbf{r})=E\psi(\mathbf{r})$. Due to polar symmetry, the following suggestion for $\psi(\mathbf{r})$ can be used

$$\psi_{nm}(\mathbf{r})=\frac{e^{im\phi}}{\sqrt{2\pi}}\frac{R_{nm}(r)}{\sqrt{r}} \tag{5}$$

with the magnetic quantum number m. If the wave function suggestion is used in the eigenvalue equation, the following differential equation is obtained

$$\frac{d^2R_{nm}(r)}{dr^2}+\frac{2m^\star}{\hbar^2}\left[E_{nm}-V_{eff}(r)\right]R_{nm}(r)=0, \tag{6}$$

with

$$V_{eff}(r)=\frac{m\hbar\omega_c}{2}+\frac{(m^2-\frac{1}{4})\hbar^2}{2m^\star r^2}+\frac{m^\star\omega_c^2}{8}r^2$$

$$+\frac{1}{2}\Big(V_{MQD}(r+\alpha_0)+V_{MQD}(r-\alpha_0)\Big)+e\xi r, \tag{7}$$

where the MQD potential is given by

$$V_{MQD}(r)=V_0\Big(sin^2(\eta r)-cos(\eta r)\Big), \tag{8}$$

where, being In-concentration x, $V_0=(1.42-1.53+0.45x^2)$ eV [73], η is the quantum dot potential width parameter. Eq. (6) is solved by using Runge–Kutta-Fehlberg(RKF) method. For details of the RKF method, please refer [74].

To specify the NOR, SHG and THG characteristics of the MQD system, it is taken into consideration that monochromatic optical radiation field ($E(t)$) having ω frequency is applied in the radial direction, and is given by

$$\mathbf{E}(t)=\tilde{\mathbf{E}}e^{i\omega t}+\tilde{\mathbf{E}}^{-i\omega t}. \tag{9}$$

The time-evolution of the matrix elements of one-electron density operator is stated as [75]

$$\frac{\partial\hat{\rho}_{ij}}{\partial t}=\frac{1}{i\hbar}[\hat{H}-\hat{M}.\mathbf{E}(t),\hat{\rho}]_{ij}-\Gamma_{ij}(\hat{\rho}-\hat{\rho}^{(0)})_{ij}, \tag{10}$$

with $\hat{\rho}$ (density matrix of one-electron system), $\hat{\rho}^{(0)}$ (unperturbed density matrix operator), $\hat{H}_0$ (the Hamiltonian of the system when no electromagnetic field), $\hat{M}.\mathbf{E}(t)=-e\hat{r}E(t)$ (perturbative contribution), Γ_{ij} (the relaxation rate in damping duration). In order to Eq. (10), the following serial solution suggestion can be considered [76]

$$\hat{\rho}(t)=\sum_{n=0}^{\infty}\hat{\rho}^{(n)}. \tag{11}$$

when considering Eq. (11), Eq. (10) is converted to the following form

$$\frac{\partial\hat{\rho}_{ij}^{(n+1)}}{\partial t}=\frac{1}{i\hbar}\left([\hat{H},\hat{\rho}^{(n+1)}]_{ij}-i\hbar\Gamma_{ij}\hat{\rho}_{ij}^{(n+1)}\right)-\frac{1}{i\hbar}[e\hat{r},\hat{\rho}^{(n)}]_{ij}E(t). \tag{12}$$

Due to $E(t)$ optical field, the electronic polarization is expressed as [77]

$$P(t)=(\varepsilon_0\chi_\omega^{(1)}\tilde{E}e^{i\omega t}+\varepsilon_0\chi_0^{(2)}\tilde{E}^2+\varepsilon_0\chi_{2\omega}^{(2)}\tilde{E}^{(2)}e^{2i\omega t}+\varepsilon_0\chi_\omega^{(3)}\tilde{E}^{(2)}\tilde{E}e^{i\omega t}$$

$$+\varepsilon_0\chi_{3\omega}^{(3)}\tilde{E}^{(3)}e^{3i\omega t}+\cdots), \tag{13}$$

where ε_0 is the permittivity of free space; $\chi_\omega^{(1)}$, $\chi_0^{(2)}$, $\chi_{2\omega}^{(2)}$, $\chi_\omega^{(3)}$ and $\chi_{3\omega}^{(3)}$ are, respectively, the linear, the optical rectification, the second harmonic generation, the third order and third harmonic generation susceptibilities. By using density-matrix approach and iterative method; NOR, SHG and THG susceptibilities are obtained in the following form [75,78]:

$$\chi_0^{(2)}=\frac{4e^3\rho_\nu}{\varepsilon_0\hbar^2}\mu_{01}^2\delta_{01}\frac{\omega_{10}^2(1+\Gamma_2/\Gamma_1)+(\omega^2+\Gamma_2^2)(\Gamma_2/\Gamma_1-1)}{[(\omega_{10}-\omega)^2+\Gamma_2^2][(\omega_{10}+\omega)^2+\Gamma_2^2]}, \tag{14}$$

$$\chi_{2\omega}^{(2)}=\frac{e^3\rho_\nu}{\varepsilon_0\hbar^2}\frac{\mu_{01}\mu_{12}\mu_{20}}{(\omega-\omega_{10}-i\Gamma_3)(2\omega-\omega_{20}-i\Gamma_3)}, \tag{15}$$

$$\chi_{3\omega}^{(3)}=\frac{e^4\rho_\nu\mu_{01}\mu_{12}\mu_{23}\mu_{30}}{\varepsilon_0\hbar^3(\omega-\omega_{10}-i\Gamma_3)(2\omega-\omega_{20}-i\Gamma_3)}\frac{1}{(3\omega-\omega_{30}-i\Gamma_3)}. \tag{16}$$

where e is the positive electron charge, ρ_ν is the electron density, $\omega_{ij}=(E_i-E_j)/\hbar$ is the transition frequency, $\Gamma_k=1/T_k$ ($k=1,2,3$) is the damping term related to lifetime of electrons in transition process. $\delta_{01}=|\mu_{00}-\mu_{11}|$ and being ψ_i initial state wave function and ψ_j final state one, $\mu_{ij}=|\langle\psi_j|r|\psi_i\rangle|$ ($i,j=0,1,2,3$) is the off-diagonal matrix elements. In consideration of the SHG, THG and NOR characteristic, the numerical setup is taken into account as $m^*=0.067m_0$ (m_0 is free electron mass), $\rho_\nu=3\times10^{23}$ m^{-3}, $\varepsilon_{GaAs}=13.18$, $\varepsilon_0=8.854\times10^{-12}$ C^2/Nm^2, $\Gamma_{1,2,3}=1.0$ Thz. The quantum dot radius is taken as $R_{dot}=6a_0$ throughout the study. The effective Rydberg energy and Bohr radius are calculated as $R_y^\star\cong5.27$ MeV and $a_0=103.7$ Å, respectively [79–81].

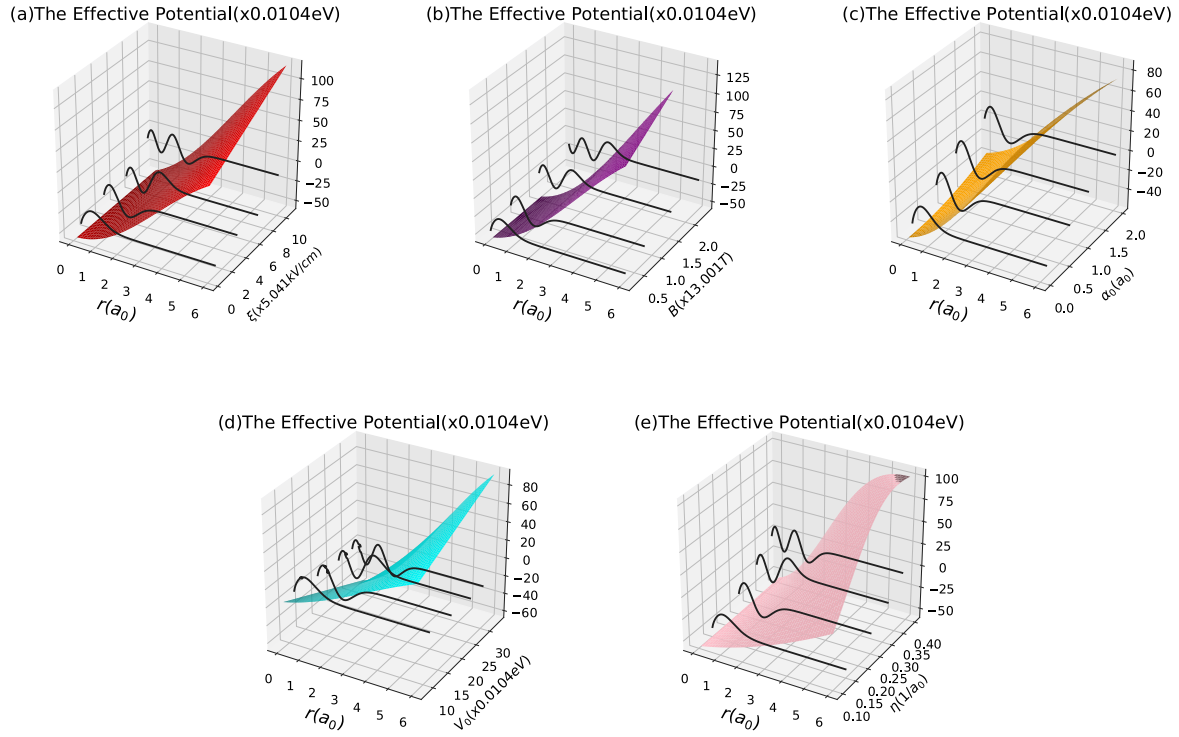

Fig. 1. The plot of the effective potential profile and first four bound state wave functions as function of the radial distance $r(a_0)$ and, (**a**) the external electric field strength (ξ(kV/cm)), when $B = 1$T, $x = 0.4$, $\eta = 0.25/a_0$, $\alpha_0 = 0.5a_0$, (**b**) the external magnetic field strength ($B(T)$), when $F = 30$ kV/cm, $x = 0.4$, $\eta = 0.25/a_0$, $\alpha_0 = 0.5a_0$, (**c**) the laser-dressed parameter ($\alpha_0(a_0)$), when $F = 30$ kV/cm, $B = 1$T, $x = 0.4$, $\eta = 0.25/a_0$, (**d**) the MQD depth depending on *In*-concentration (x), when $F = 30$ kV/cm, $B = 1$T, $x = 0.4$, $\eta = 0.25/a_0$, $\alpha_0 = 0.5a_0$, (**e**) the MQD width parameter ($\eta(1/a_0)$), when $F = 30$ kV/cm, $B = 1$T, $x = 0.4$, $\eta = 0.25/a_0$, $\alpha_0 = 0.5a_0$.

3. Result and discussions

In this work, the effects of structure parameters such as In−concentration (x) and quantum dot width (η) on nonlinear optical properties such as the NOR, SHG and THG of the Mathieu quantum dot (MQD) under the influence of the electric field (ξ), magnetic field (B) and laser field (α_0) are examined. For the first four electronic energy levels, the effective potential and the relevant wave functions are presented as a function of the radial distance (r) and the electric field in Fig. 1a, the magnetic field in Fig. 1b, the laser radiation field in Fig. 1c, the potential depth in Fig. 1d, the width of the MQD in Fig. 1e.

Fig. 2a, b, and c demonstrate, respectively, the variation of the NOR, SHG and THG of the MQD in consideration of certain constant values of the structure parameters and other external field parameters, depending on the applied external electric field. As the applied external electric field increases, as seen in Fig. 1a, the repulsiveness of the effective potential increases, which enhances the difference between the bound state energy levels. This situation is confirmed in Fig. 2a inset, which depicts the variation of energy levels with respect to the electric field. As can be seen in Fig. 2a inset, the difference between energy levels ($\Delta E = E_1 - E_0$) increases with increasing electric field. Because the applied electric field breaks the symmetry of the structure. Increasing the difference between the energy levels causes the NOR resonant frequencies to be blue-shifted. Another remarkable point in Fig. 2a is that the NOR amplitudes decrease due to the increasing electric field. This situation can be explained by the variation of the dipole matrix elements depending on the electric field. It can be seen in Fig. 2a inset that $\mu^{\times} = \mu_{01}^2 \delta_{01}$ decreases as the electric field increases. The variation of matrix elements ($\mu^{\times} = \mu_{01}^2 \delta_{01}$) versus the change of the electric field dominates over the variation of the NOR amplitudes with electric field. Therefore, as the electric field increases, the NOR amplitudes decrease in Fig. 2a. In Fig. 2b, the variation of the SHG coefficients $\chi_{2\omega}^{(2)}$ is presented depending on the incident photon energy for different electric field strengths. Since the electric field breaks the symmetry of the MQD (Fig. 1a), it triggers the SHG effects. The first noteworthy point in Fig. 2b is that two distinct resonant peaks 2ω of $\chi_{2\omega}^{(2)}$ have been observed. The larger one of these two peaks occurs around $\hbar\omega = E_1 - E_0$, while the smaller peak one occurs around approximately $\hbar\omega = (E_2 - E_0)/2$. As the electric field value decreases, it is seen that two peaks formed in the SHG coefficients turn into a sharp single peak. This is because when $\hbar\omega = (E_2 - E_0)/2 \approx E_1 - E_0$, the double resonant comes true and then a sharp peak occurs. As the electric field decreases, we can say that the probability of creating frequency dubbing of the structure increases. It is also seen that the SHG resonant frequencies shift to the blue as the electric field increases, and this shift is due to the new localizations arising from the strengthened electric field (Fig. 2b inset (ΔE)). The SHG amplitude decreases because of applied electric field. The reason for this decrement in amplitude is the variation with the electric field of the matrix elements ($\mu^{\times} = \mu_{01}\mu_{12}\mu_{20}$) presented in Fig. 2b. Fig. 2c furnishes the variation of the THG coefficients ($\chi_{3\omega}^{(3)}$) depending on the incident photon energy at different electric field values. Depending on the applied electric field, we can say that the tendency of the THG coefficients is similar to that of the SHG coefficients. Three different peaks values in the THG resonant peaks at $\xi = 30$ kV/cm and $\xi = 90$ kV/cm are observed, one of them is very faint. The highest one of these peaks forms around $\Delta E = (E_3 - E_0)/3$ resonant energy value, the peak to the left of this peak is at $\Delta E = (E_2 - E_0)/2$, while the weakest one is at $\Delta E = E_1 - E_0$. However, it is seen that the third peak constituting the weakest peak in the THG profile does not occur at $\xi = 10$ kV/cm. Because, as the energy levels converge, a double resonance situation has occurred here. When $\xi = 1$ kV/cm, only one resonant peak is observed. The reason for this is the formation of triple resonant peak for the THG coefficients at this value. It can be said that as the electric field increases, the symmetry of the structure modifies and the bound states move away from each other, and then the probability of occurrence for the THG resonant peaks increases. As can be seen in Fig. 2c, as the electric field increases, the THG resonant frequencies shift to blue, which is because $\Delta E = (E_3 - E_0)$ increases with

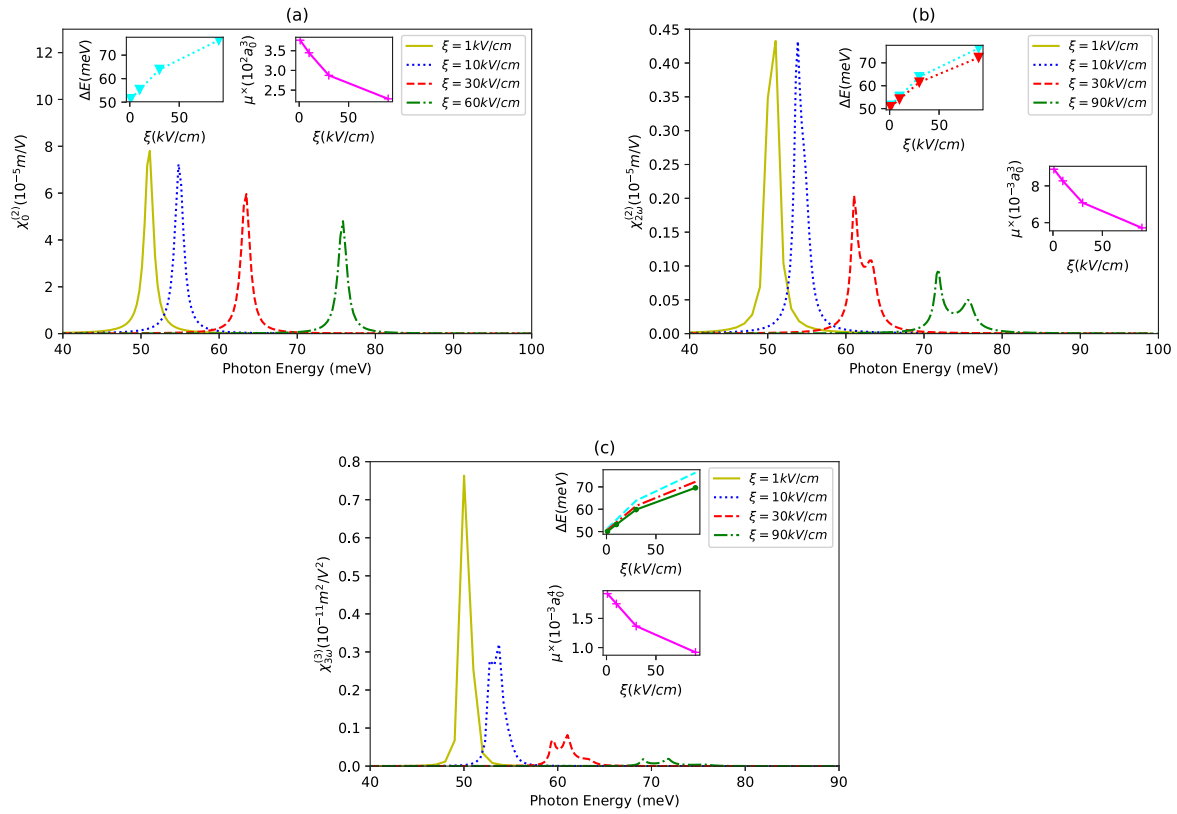

Fig. 2. The NOR (panel **a**), SHG (panel **b**) and THG coefficients (panel **c**) of the MQD with $\xi = 1-10-30-60$ kV/cm, $B = 1$T, $x = 0.4$, $\eta = 0.25/a_0$, $\alpha_0 = 0.5a_0$. The insets show the relevant energy differences and matrix elements, respectively; as $\Delta E = E_1 - E_0$ (cyan) and $\mu^{\times} = \mu_{01}^2\delta_{01}$ for the NOR coefficients (panel **a**), $\Delta E = (E_2 - E_0)/2$ (red) and $\mu^{\times} = \mu_{01}\mu_{12}\mu_{20}$ for the SHG coefficients (panel **b**), $\Delta E = (E_3 - E_0)/3$ (green) and $\mu^{\times} = \mu_{01}\mu_{12}\mu_{23}\mu_{30}$ for the THG coefficients (panel **c**).

the increasing the electric field (See Fig. 2c inset). The THG amplitude decreases with the applied electric field. This decrease is consistent with the variation of the matrix elements $\mu^{\times} = \mu_{01}\mu_{12}\mu_{23}\mu_{30}$.

The NOR, SHG and THG characteristics of the MQD are, respectively, represented as a function of the incident photon energy for different external magnetic field values in Fig. 3a, b and c. It is seen in Fig. 3a that the NOR resonant frequencies shift to blue as the magnetic field increases. This is due to the magnetic field-dependent variation of the effective potential profile in Fig. 1b. As can be seen in Fig. 1b, the repulsiveness of the MQD becomes clear with increasing magnetic field. This change in potential increases the difference between the bound state localizations (See Fig. 3a inset). In addition, the increasing magnetic field causes a decrement in the NOR amplitudes, which is due to the variation of the matrix elements ($\mu^{\times}$) with the magnetic field (See Fig. 3a inset). In Fig. 3b, the SHG change is presented depending on the incident photon energy for different magnetic field values. As can be observed in Fig. 3b inset that the SHG resonant frequencies shift to blue as result of the increment of the energy difference with the increasing magnetic field. In Fig. 3b, it should be pointed out that the matrix elements ($\mu^{\times}$) do not dominate on the SHG amplitudes (See Fig. 3b inset). When considering Eq. (15), the SHG amplitudes change with a form in which resonant frequencies are also active as well as matrix elements. On the other hand, it is observed that the increment of the magnetic field does not change the SHG character, that is, double peaks always occur. Therefore, it can be said that the increment of the magnetic field does not affect the stability of the SHG character of the MQD. In Fig. 3c, it is seen that the THG resonant frequencies display the blue-shift as the magnetic field increases. Because the augment of the magnetic field increases ΔEs (See Fig. 3c inset), which is due to the increase in the energy difference between localizations as a result of the repulsion arising from the magnetic field in the potential profile (See Fig. 3c). As seen, the variation of THG amplitudes exhibits a fluctuation, and upon this fluctuation, the only matrix elements are not dominant alone (See Fig. 3c inset). This fluctuation does not arise from not only by the matrix elements, but also by a form in which the transition frequencies are active.

In Fig. 4a, b and c, the variation of the NOR, SHG and THG of the MQD depending on the applied laser field is, respectively, demonstared as a function of the incident photon energy. As seen in Fig. 1c, as the applied laser field strength increases, the effective potential depth decreases while its width increases, which leads to the decrement of the energy difference between bound state localizations (See Fig. 4a inset). This decrement triggers to the red-shifting in the NOR resonant frequencies. It is important to note in Fig. 4a that the increasing laser field strength enhances slightly the NOR amplitudes. In Fig. 4a inset, there is a parallelism between the increase of dipole matrix elements ($\mu^{\times}$) and the increment of NOR amplitudes. In this case, it can be said that the laser field strength is dominant for the NOR amplitudes. In Fig. 4b, the variation of the SHG coefficients is shown depending on the incident photon energy for different laser field strengths. Similar to the previous discussions, two different resonant SHG peaks are observed at two different energy values under the laser field effect. As seen in Fig. 4b, due to the augment in laser field strength, the SHG resonant frequencies shift to red as a result of localizations in the new potential profile. When analysing the amplitudes by considering laser field, it is seen that the small resonant peaks formed at $\hbar\omega = (E_2 - E_0)/2$ enhance in line with change by the laser field of the matrix elements depending on the increasing laser field (See Fig. 4(b) inset, the change graph of matrix elements with laser field), but the large peak amplitudes around $\hbar\omega = (E_1 - E_0)$ are not compatible with matrix elements. Generally speaking, the fluctuation in the SHG amplitudes is influenced not only by the matrix elements ($\mu^{\times}$) but also by a different form including the resonant frequencies. In Fig. 4c, the variation of THG coefficients is given depending on the incident photon energy for different laser field

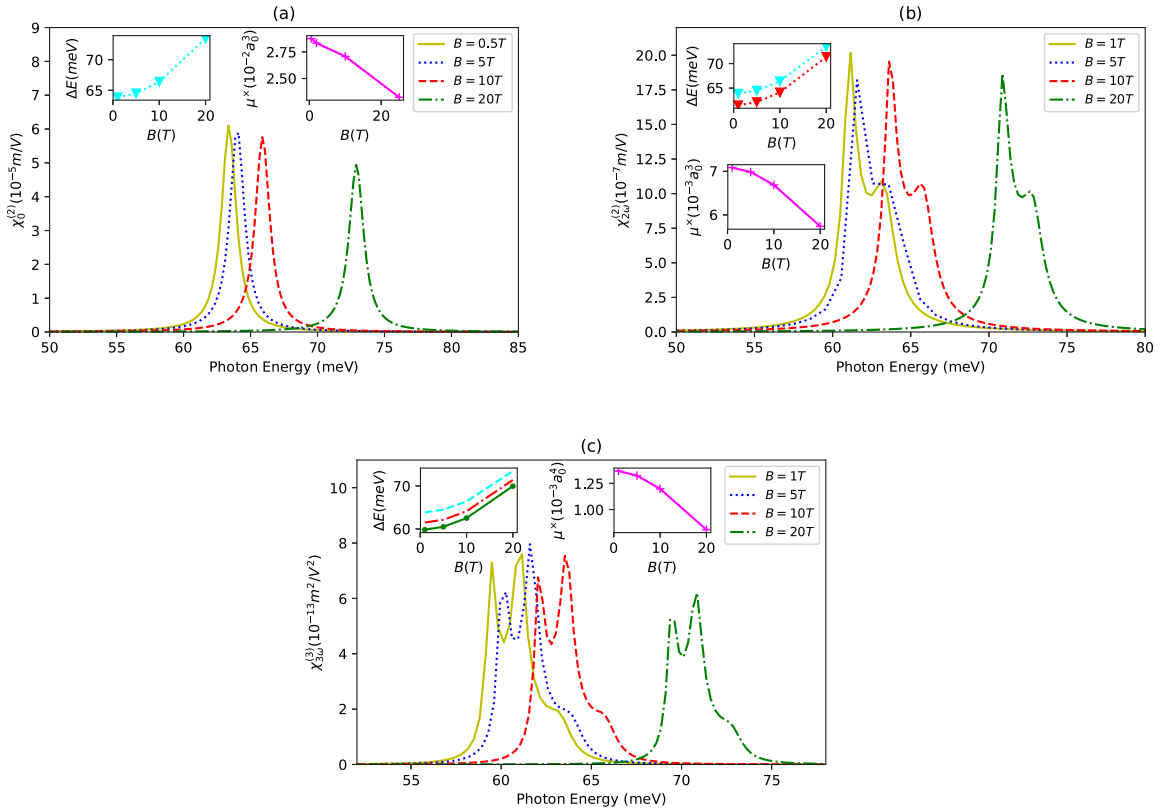

Fig. 3. The same as Fig. 2 but when $\xi = 30$ kV/cm, $B = 1 - 5 - 10 - 20$T, $x = 0.4$, $\eta = 0.25/a_0$, $\alpha_0 = 0.5a_0$.

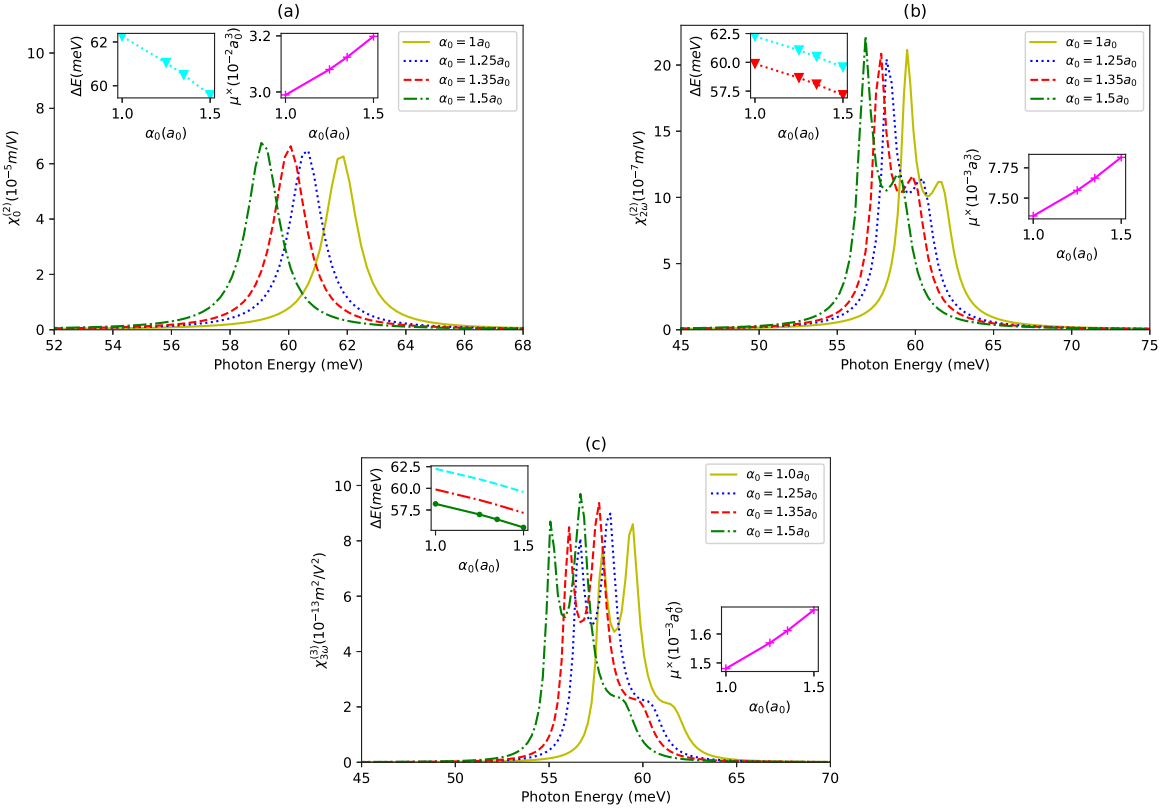

Fig. 4. The same as Fig. 2 but when $\xi = 30$ kV/cm, $B = 1$T, $x = 0.4$, $\eta = 0.25/a_0$, $\alpha_0 = 1 - 1.25 - 1.35 - 1.5a_0$.

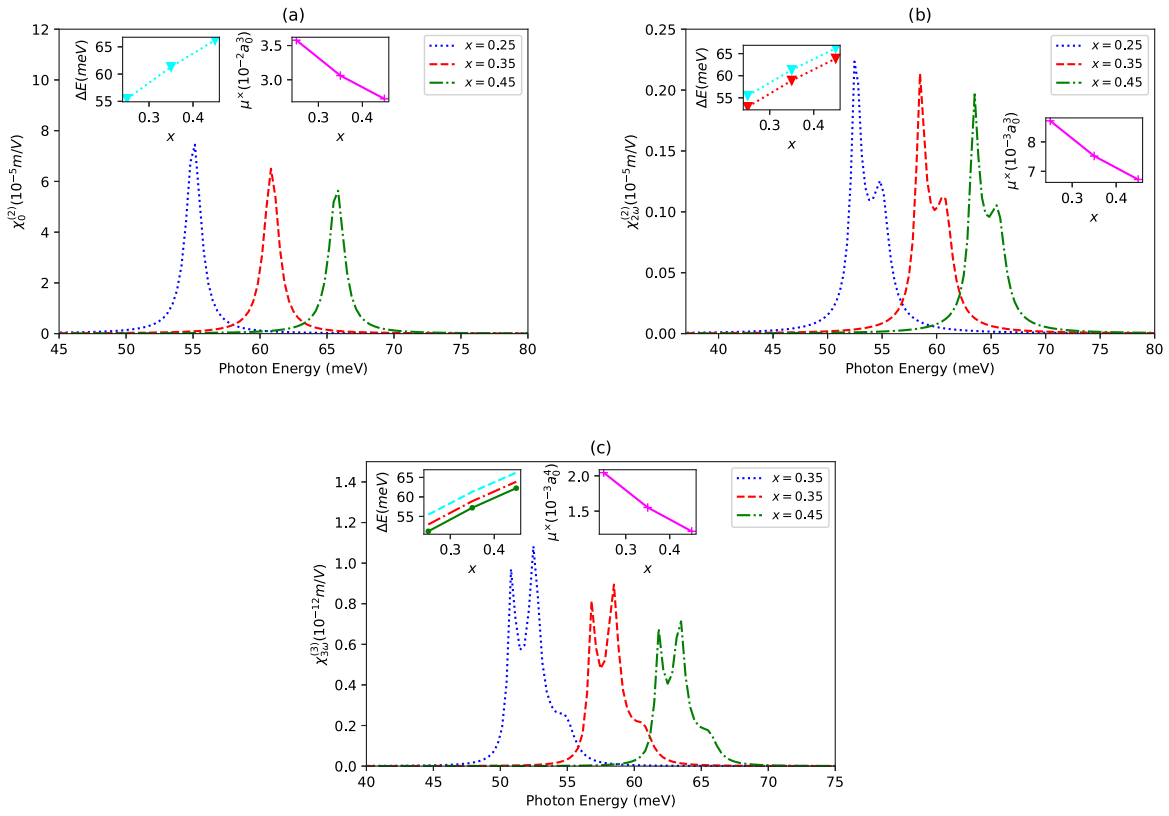

Fig. 5. The same as Fig. 2 but when $\xi = 30$ kV/cm, $B = 1$T, $x = 0.15 - 0.25 - 0.35 - 0.45$, $\eta = 0.25/a_0$, $\alpha_0 = 0.5a_0$.

strengths. As explained in previous discussions, three resonant peaks occur. Due to the increased laser field, the THG resonant frequencies shift to red as a result of new localizations as elucidated previously, which is confirmed in Fig. 4c inset (ΔE). Also, it is clear that the variation of the matrix elements with only laser field is not effective alone on the THG peak amplitudes.

In Fig. 5a, b and c, the NOR, SHG and THG of the MQD are given for different In−concentration values as $x = 0,25$, $x = 0.35$ and $x = 0.45$, as a function of the incident photon energy. In Fig. 5a, it is seen that NOR resonant frequencies shift to blue as x increases, this is due to the increase in effective potential depth as x increases. As the attractiveness of the potential increases, the energy difference between the bound state localizations increases, which is confirmed in Fig. 5a inset. Also, the NOR amplitudes decrease (Fig. 5a inset) as matrix elements ($\mu^{\times}$) decrease with increasing x value. In Fig. 5b, when examining the variation of the SHG coefficients depending on the x concentration, it is observed that as x increases, the SHG resonant peaks shift to blue and the resonant amplitudes decrease. Maximum peak values are observed at two different frequency values in agreement with the SHG coefficients. The reason for this change is the energy differences and the variation of the matrix elements depending on x, as elucidated in the NOR change. In Fig. 5c, it is seen that the THG resonant frequencies shift to blue and their amplitudes decrease as x increases, similar to the NOR and SHG coefficients, the reason to which is as described in the SHG and NOR characters. Again, as expected, the THG resonant peaks occur at appropriate ΔE values as $(E_1 - E_0)$, $(E_2 - E_0)/2$ and $(E_3 - E_0)/3$.

In Fig. 6a, b and c, respectively, the NOR, SHG and THG of the MQD are furnished for different width parameter values (η) of the quantum dot as a function of the incident photon energy. As seen in Fig. 6a, as η increases, the NOR resonant frequencies shift to blue, while resonant amplitudes decrease. Because, in Fig. 1, it is seen that as the η value increases, the repulsiveness of the effective potential increases. In this case, the difference between the bound state energies increases, and the NOR resonant frequencies begin to blue-shifting (See Fig. 6a inset). Also, the NOR amplitudes decrease (See Fig. 6a inset) as matrix elements ($\mu^{\times}$) decrease with increasing η value. When probing the variation of the SHG coefficients in Fig. 6b and the THG coefficients in Fig. 6c with respect to η, it is observed that SHG and THG coefficients blueshift similar to the NOR resonant frequencies due to the increasing η. The reason for this observation can be elucidated by the fact that the energy difference increases as η increases (See Fig. 6b inset and Fig. 6c inset). Also, it is seen in Fig. 6b and c, respectively, that the resonant amplitudes of the SHG and THG coefficients decrease as η increases, which is due to decrement of the dipole matrix elements ($\mu^{\times}$) as a result of increasing η (See Fig. 6b inset and Fig. 6b inset).

4. Concluding remarks

In this work, the effects of external fields such as the electric field, magnetic field, and laser field, as well as structural parameters as QD depth and width, on the NOR, SHG, and THG of the MQD constituted by $In_xGa1xAs/GaAs$ heterostructure have been theoretically investigated. From the observed results, it can be said that ξ, B, x, and η have alternative effects on the NOR, SHG, and THG resonant frequencies due to their similar blue shift function. However, in this alternative, the parameters have different efficacy relative to each other. While the external electric field changes the SHG and THG stability of the MQD, the external magnetic field, laser field and structure parameters do not change this stability. Because only the external electric field increase causes a sharp peak formation in SHG and THG characters. In summary, both external fields and structural parameters are influential in the optical responses of the structure. The determination of the functional ranges of these parameters through the theoretically calculated effects will provide advantages in the experimental stage for the production of planned optoelectronic devices. The applied external electric field serves as an alternative to structural parameters in terms of both optimality and resonant frequencies. Furthermore, in terms of resonant frequencies, the laser field and external parameters are alternative to

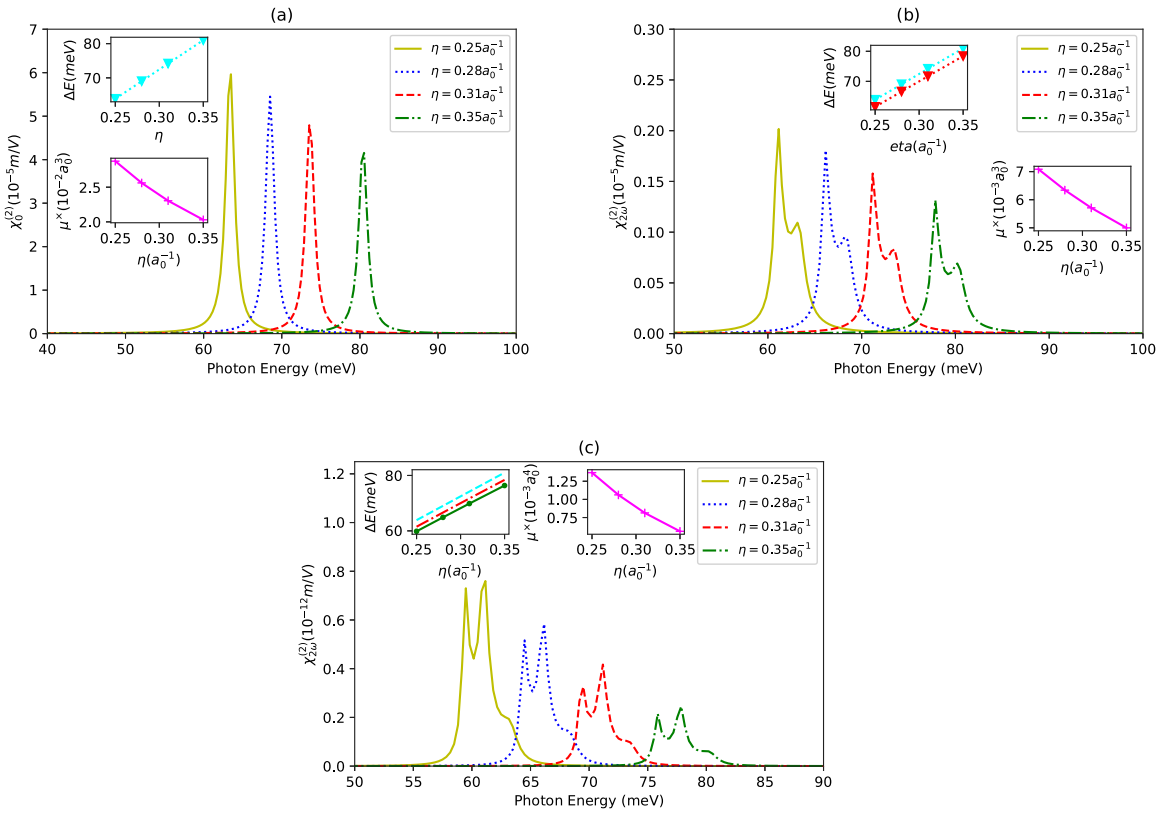

Fig. 6. The same as Fig. 2 but when $\xi = 30$ kV/cm, $B = 1$T, $x = 0.4$, $\eta = 0.25 - 0.28 - 0.31 - 0.35/a_0$, $\alpha_0 = 0.5a_0$.

each other. The relevant alternatives will provide considerable advantages for device designs in determining the nonlinear optical properties of the MQD, which resemble periodic multi-quantum wells, that can be obtained using greater spatial limitation via advanced experimental techniques.

CRediT authorship contribution statement

Mustafa Kemal Bahar: Conception and design of study, Acquisition of data, Analysis and/or interpretation of data, Writing – original draft, Writing – review & editing. **Pınar Başer:** Analysis and/or interpretation of data, Writing – original draft.

Declaration of competing interest

The authors declare that they have no known competing financial interests or personal relationships that could have appeared to influence the work reported in this paper.

Funding no

No funding was received for conducting this study. All authors approved the version of the manuscript to be published.

Code availability

Not applicable.

Data availability

No data was used for the research described in the article

References

[1] A.D. Yoffe, Low-dimensional systems: quantum size efects and electronic properties of semiconductor microcrystallites (zero-dimensional systems) and some quasi-two-dimensional systems, Adv. Phys. 42 (1993) 173.

[2] V.M. Axt, S. Mukamel, Nonlinear optics of semiconductor and molecular nanostructures; a common perspective, Rev. Modern Phys. 70 (1998) 145.

[3] L.W. Tutt, T.F. Boggess, A review of optical limiting mechanisms and devices using organics, fullerenes, semiconductors and other materials, Prog. Quant. Electron. 17 (1993) 299.

[4] J. Wang, W.J. Blau, Inorganic and hybrid nanostructures for optical limiting, J. Opt. A: Pure Appl. Opt. 11 (2009) 024001.

[5] A.L. Stepanov, Nonlinear optical properties of implanted metal nanoparticles in various transparent matrixes: A review, Rev. Adv. Mater. Sci. 27 (2011) 115.

[6] S. Lee, R. Arefin, H. Jung, et al., Morphological and optical characterization of self-assembled InAlGaAs/GaAs quantum dots, J. Appl. Phys. 131 (2022) 233104.

[7] P. Hosseinpour, A. SoltaniVala, J. Barvestani, Effect of impurity on the absorption of a parabolic quantum dot with including rashba spin–orbit interaction, Physica E 80 (2016) 48.

[8] L. Zhang, X. Li, X. Liu, Z. Li, The influence of second-harmonic generation under the external electric field and magnetic field of parabolic quantum dots, Physica B 618 (2021) 413197.

[9] A. Abdollahinia, S. Banyoudeh, A. Rippien, F. Schnabel, O. Eyal, I. Cestier, I. Kalifa, E. Mentovich, G. Eisenstein, J.P. Reithmaier, Temperature stabil-ity of static and dynamic properties of 1.55 μm quantum dot lasers, Opt. Express Express 26 (2018) 6056.

[10] H. Huang, J. Duan, D. Jung, A.Y. Liu, Z. Zhang, J. Norman, J.E. Bowers, F. Grillot, Analysis of the optical feedback dynamics in InAs/GaAs quantumdot lasers directly grown on silicon, J. Opt. Soc. Amer. B 35 (2018) 2780.

[11] N. Ledentsov, V.M. Ustinov, V.A. Shchukin, P.S. Kop'Ev, Z.I. Alferov, D. Bimberg, Quantum dot heterostructures: Fabrication, properties, lasers, Semiconductors 32 (1998) 343.

[12] T. Septon, A. Becker, S. Gosh, G. Shtendel, V. Sichkovskyi, F. Schnabel, A. Sengül, M. Bjelica, B. Witzigmann, J.P. Reithmaier, Large linewidthreduction in semiconductor lasers based on atom-like gain material, Optica 6 (2019) 1071.

[13] S. Md Arif, A. Bera, A. Ghosh, M. Ghosh, Analyzing role of relaxation time on second harmonic generation and optical dielectric function of impurity doped quantum dots under the aegis of noise, Physica B 588 (2020) 412166.

[14] H.V. Phuc, D.Q. Khoa, N. VanHieu, N.N. Hieu, Linear and nonlinear magneto-optical absorption in parabolic quantum well, Optik 127 (22) (2016) 10519.

[15] J. Ge, S. Han, X. Miao, Y. Sun, J. Xiao, Asymmetrical gaussian potential effects on strongly coupled magnetopolaron properties in triangular confinement potential quantum wells, Coatings 12 (12) (2022).

[16] C. Carib, A. Suparmia, S. Faniandaric, Solution of Schrödinger equation for screened modified pöschl-teller potential in spherical quantum dots and its application in linear and nonlinear optical properties, AIP Conf. Proc. 2391 (2022) 090009.

[17] C. Cai, X. Ma, C. Zhao, J. Xiao, Impurity effect on the ground state binding energy of a fully coupled polaron in a double ring shaped quantum dot, Physica B 632 (2022) 413699.

[18] F.M. Peeters, Magneto-optics in parabolic quantum dots, Phys. Rev. B 42 (1990) 1486(R).

[19] J.H. Davies, The Physics of Low-Dimensional Semiconductors: An Introduction, fifth ed., Cambridge, USA, 1999.

[20] E. Mathieu, Memoire sur le mouvement vibratoire d'une membrane de forme elliptique, J. Math. Pures Appl. 13 (1868) 137.

[21] H. Garcia-Gracia, J.C. Gutierrez-Vega, Polarization singularities in nondiffracting Mathieu–Poincaré beams, J. Opt. 18 (2016) 014006.

[22] F.M. Arscott, Periodic Differential Equations: An Introduction to Mathieu, LamÉ, and Allied Functions, Pergamon Press, ISBN: 9781483164885, 1964.

[23] R. Barakat, Diffraction of plane waves by an elliptic cylinder, J. Acoust. Soc. Am. 35 (1963) 1990.

[24] J. Meixner, F. Schafke, Wilhelm Mathieusche Funktionen und SphÄroidfunktione (in German), Springer-Verlag, Berlin, 1954.

[25] M.M. Bibby, A.F. Peterson, Accurate Computation of Mathieu Functions Synthesis Lectures on Computational Electromagnetics, Morgan and Claypool, ISBN: 9781627050852, 2014.

[26] A. Sebak, L. Shafai, Generalized solutions for electromagnetic scattering by elliptical structures, Comput. Phys. Comm. 68 (1991) 315.

[27] L. Ruby, Applications of the Mathieu equation, Amer. J. Phys. 64 (1996) 39.

[28] J. Meixner, F.W. Schafke, Mathieusche Funktionen und Spharoidfunktionen Mit Anwendungen auf Physikalische und Technische Probleme, Springer-Verlag, ISBN: 978-3-540-01806-3, 1954.

[29] R.E. March, An introduction to quadrupole ion trap mass spectrometry, J. Mass Spectr. 32 (4) (1997) 351.

[30] R.W. Robinett, The stark effect in linear potentials, Quant. Phys. 1 (2009).

[31] C. Brimacombe, R. Corless, M. Zamir, Computation and applications of Mathieu functions: A historical perspective, SIAM Rev. 63 (4) (2021) 653.

[32] D.J. Daniel, Exact solutions of Mathieu's equation, Prog. Theor. Exp. Phys. 4 (2020) 043A01.

[33] T. Pearsall, Ga0.47In0.53As: A ternary semiconductor for photodetector applications, IEEE J. Quant. Electron. Inst. Electr. Electron. Eng. (IEEE) 16 (7) (1980) 709.

[34] R.J. Nicholas, J.C. Portal, C. Houlbert, P. Perrier, T.P. Pearsall, An experimental determination of the effective masses for $Ga_xIn_{1-x}As_yP_{1-y}$ alloys grown on InP, Appl. Phys. Lett. 34 (8) (1979) 492.

[35] T.P. Pearsall, M.A. Pollack, W.T. Tsang, Photodiodes for optical fiber communication, Semicond. Semimetals 17 (1985) 174.

[36] K. Alavi, H. Temkin, A.Y. Cho, T.P. Pearsall, AlInAs-GaInAs multi quantum-well lasers emitting at 1.55 μm, Appl. Phys. Lett. 4244 (1983) 845.

[37] J. Faist, Quantum Cascade Laser, Oxford University Press, Oxford, 2013.

[38] J. Kwoen, T. Imoto, Y. Arakawa, InAs/InGaAs quantum dot lasers on multi-functional metamorphic buffer layers, Opt. Express 29 (2021) 29378.

[39] M. Tan, L. Ji, Y. Wu, P. Dai, Q. Wang, K. Li, T. Yu, Y. Yu, S. Lu, H. Yang, Investigation of InGaAs thermophotovoltaic cells under blackbody radiation, Appl. Phys. Express 7 (2014) 096601.

[40] H.L. Hao, M.Y. Su, H.T. Wu, H.Y. Mei, R.X. Yao, F. Liu, H. Wen, S.X. Sun, Influence of double InGaAs/InAs channel on DC and RF performances of InP-based HEMTs, J. Ovonic Res. 18 (2022) 411.

[41] A.A. Naghmaish, H. Dakhlaoui, T. Ghrib, B.M. Wong, Effects of magnetic, electric, and intense laser fields on the optical properties of AlGaAs/GaAs quantum wells for terahertz photodetectors, Phys. B 635 (2022) 413838.

[42] E. Rosencher, P. Bois, Model system for optical nonlinearities: Asymmetric quantum wells, Phys. Rev. B 44 (1991) 11315.

[43] I. Karabulut, H. Safak, M. Tomak, Linear and nonlinear intersubband optical absorptions in an asymmetric rectangular quantum well, Solid State Commun. 135 (2005) 735.

[44] G.J. Zhao, X.X. Liang, S.L. Ban, Binding energies of donors in quantum wells under hydrostatic pressure, Phys. Lett. A 319 (2003) 191.

[45] H. Dakhlaoui, Tunability of the optical absorption and refractive index changes in step-like and parabolic quantum wells under external electric field, Optik 168 (2018) 416.

[46] A. AL-Naghmaish, H. Dakhlaoui, T. Ghrib, B.M. Wong, Effects of magnetic, electric, and intense laser fields on the optical properties of AlGaAs/GaAs quantum wells for terahertz phodetectors, Physica B 635 (2022) 413838.

[47] F. Ungan, M.K. Bahar, Optical specifications of laser-induced Rosen–Morse quantum well, Opt. Mater. 90 (2019) 231.

[48] S. Aktaş, A. Bilekkaya, F.K. Boz, S.E. Okan, Electron transmission in symmetric and symmetric double-barrier structures controlled by laser fields, Superlatt. Microstruct. 85 (2015) 266.

[49] R.Y. Yan, J. Tang, Z.H. Zhang, Optical properties in GaAs/AlGaAs semiparabolic quantum wells by the finite difference method: combined effects of electric field and magnetic field, Internat. J. Modern Phys. B 32 (2018) 1850159.

[50] E.C. Niculescua, L.M. Burileanu, Nonlinear optical absorption in inverse V-shaped quantum wells modulated by high-frequency laser field, Eur. Phys. J. B 74 (2010) 117.

[51] G.P. Agrawal, Applications of Nonlinear Fiber Optics, Academic Press, 2019.

[52] R.K. Srivastav, A. Panwar, Excitation of terahertz surface magnetoplasmons by nonlinear mixing of two lasers on a rippled surface of magnetized n-InSb, Optik 264 (2022) 169363.

[53] U.K. Sapaev, I.A. Kulagin, T. Usmanov, Theory of second-harmonic generation for limited laser beams in nonlinear crystals, J. Opt. B 5 (2003) 355.

[54] P. Wasylczyk, I.A. Walmsley, W. Wasilewski, C. Radzewicz, Broadband noncollinear optical parametric amplifier using a single crystal, Opt. Lett. 30 (2005) 1704.

[55] P.J. Campagnola, A.C. Millard, M. Terasaki, P.E. Hoppe, C.J. Malone, W.A. Mohler, Three-dimensional high-resolution second-harmonic generation imaging of endogenous structural proteins in biological tissues, Biophys. J. 82 (2002) 493.

[56] R.A. Ganeev, V.V. Kim, I.A. Shuklov, V.S. Popov, N.A. Lavrentyev, V.P. Ponomarenko, A.A. Mardini, D.V. Dyomkin, T. Milenkovic, A. Bundulis, J. Grube, A. Sarakovskis, Third harmonic generation in the thin films containing quantum dots and exfoliated nanoparticles, Appl. Phys. B 128 (2022) 202.

[57] D. Bejan, E.C. Niculescu, Electronic and optical properties of asymmetric GaAs double quantum dots in intense laser fields, Phil. Mag. 96 (2016) 1131.

[58] R. Khordad, A. Ghanbari, K. Abbasi, A. Ghafaripour, Harmonic generation of tuned quantum dots including impurity efects, J. Comput. Electron. J. Comput. Electron. 1 (2022) 260.

[59] S. Baskoutas, E. Paspalakis, A.F. Terzis, Electronic structure and nonlinear optical rectification in a quantum dot: effects of impurities and external electric field, J. Phys.: Condens. Matter 19 (2007) 395024.

[60] K. Li, S. Zhu, S. Dai, Z. Li, H. Yin, Z. Chen, Shape effect on the electronic state and nonlinear optical properties in the regulable Y-shaped quantum dots under applied electric field, Opt. Express 29 (2021) 5849.

[61] T.A. Sargsian, P.A. Mantashyan, D.B. Hayrapetyan, Effect of Gaussian and Bessel laser beams on linear and nonlinear optical properties of vertically coupled cylindrical quantum dots, Nano-Struct. Nano-Objects 33 (2023) 100936.

[62] S. Pal, M. Ghosh, Tailoring nonlinear optical rectification coefficient of impurity doped quantum dots by invoking Gaussian white noise, Opt. Quantum Electron. 48 (2016) 372.

[63] J. Ganguly, M. Ghosh, Modulating optical second harmonic generation of impurity-doped quantum dots in presence of Gaussian white noise, Phys. Status Solidi B 253 (2016) 1093.

[64] S. Saha, M. Ghosh, Tuning third harmonic generation of impurity doped quantum dots in the presence of Gaussian white noise, J. Phys. Chem. Solids 90 (2016) 69.

[65] J. Ganguly, S. Saha, A. Bera, M. Ghosh, Modulating optical rectification, second and third harmonic generation of doped quantum dots: Interplay between hydrostatic pressure, temperature and noise, Superlattices Microstruct. 98 (2016) 385.

[66] B.H. Bransden, C.J. Joachain, Physics of Atoms and Molecules, Prentice-Hall, Upper Saddle River, NJ, USA, 2003.

[67] M. Gavrila, J.Z. Kaminski, Free-free transitions in intense high-frequency laser fields, Phys. Rev. Lett. 52 (1984) 613.

[68] W.C. Henneberger, Perturbation method for atoms in intense light beams, Phys. Rev. Lett. 21 (1968) 838.

[69] H.A. Kramers, Collected Scientific Paper, North-Holland, Amsterdam, The Netherlands, 1956, p. 866.

[70] F. Ehlotzky, Scattering phenomena in strong radiation fields II, Can. J. Phys. 63 (1985) 907.

[71] F. Ehlotzky, Positronium decay in intense high frequency laser fields, Phys. Lett. A 126 (1988) 524.

[72] P. Harrison, Quantum Wells, Wires, Dots, second ed., Wiley, UK, 2005.

[73] S. Adachi, Physical Properties of III-V Semiconductor Compounds, A Wiley-Interscience Publication, John Wiley and Sons, 1992.

[74] K. Kılıç, M.K. Bahar, Optical response of plasma processed quantum dot under the external fields, Int. J. Quantum Chem. 121 (2021) e26564.

[75] Y.B. Yu, H.J. Wang, Third-harmonic generation in two-dimensional pseudo-dot system with an applied magnetic field, Superlattices Microstruct. 50 (2011) 252.
[76] E. Rosencher, Model system for optical nonlinearities: asymmetric quantum wells, Phys. Rev. B 252 (1991) 44.
[77] G. Rezaei, B. Vaseghi, F. Taghizadeh, M.R.K. Vahdani, M.J. Karimi, Intersubband optical absorption coefficient changes and refractive index changes in a two-dimensional quantum pseudodot system, Superlattices Microstruct. 48 (2010) 450.
[78] R.W. Boyd, Nonlinear Optics, third ed., Rochester, New York, 2007.
[79] S. Paul, J.B. Roy, P.K. Basu, Empirical expressions for the alloy composition and temperature dependence of the band gap and intrinsic carrier density in $Ga_x In_{1-x}As$, J. Appl. Phys. 69 (1991) 827.
[80] F. Ungan, M.K. Bahar, M.G. Barseghyan, L.M. Perez, D. Laroze, Effect of intense laser and electric fields on nonlinear optical properties of cylindrical quantum dot with Morse potential, Optik 236 (2021) 16662.
[81] P. Başer, M.K. Bahar, Evaluation of the external electric- and magnetic field-driven Mathieu quantum dot's optical observables, Physica B 639 (2022) 413991.